




Effect of Ni on the wetting and brazing characterization of 304 stainless steel by Ag–Cu alloy

Guoqian Mu¹, Wenqing Qu^{1,*} , Yanhua Zhang¹, and Hongshou Zhuang¹

¹ School of Mechanical Engineering and Automation, Beihang University, Beijing 100191, China

Received: 4 November 2022

Accepted: 5 March 2023

Published online:
1 April 2023

© The Author(s), under exclusive licence to Springer Science+Business Media, LLC, part of Springer Nature 2023

ABSTRACT

The effect of Ni in Ag–Cu filler on the wetting and brazing characterization of stainless steel was studied by means of wetting test and brazing test under high vacuum condition. The wettability of filler metal and the joint strength were improved after adding Ni in Ag–Cu filler. The filler penetrates into stainless steel and the topmost steel grains separate from the substrate, exposing the metal surface without oxide film after adding Ni, which leads to the reduction in contact angle. The interdiffusion between FM and SS is enhanced after adding Ni, which leads to further reduction in contact angle. At wetting temperature, large amount of Ni in liquid enriched at solid–liquid interface, increasing the Cu content in liquid near the interface to form Cu-rich liquid, which caused the penetration of liquid filler. Cu first penetrates into steel grain boundary, which provides a path for Ni diffusion into stainless steel. After the oxide film was removed, a large number of Ni directly diffused into stainless steel to form (γ -Fe, Ni) layer on stainless steel surface. Cu in liquid can directly diffuse into (γ -Fe, Ni). Stainless steel can dissolve in Cu-rich liquid with high Ni content. In the absence of Ni, FM/SS interface is the weakest location of the joint. After adding Ni in filler, the formation of Cu solid solution at FM/SS interface and the enhancement of interdiffusion between FM and SS strengthen the FM/SS interface, leading to the increase in joint strength. The results in this paper suggest Ni is beneficial for brazing stainless steel by Ag–Cu alloy.

Introduction

Due to the excellent formability, corrosion and high temperature resistance, austenitic stainless steel (ASS) is widely used in energy, nuclear, electronics,

machinery, chemical industry, life fields and even some highly complex products. Brazing is widely used in manufacturing parts with complex-shape and is suitable for joining dissimilar materials. In particular, vacuum brazing can obtain clean joints without the use of flux. At present, a large number of filler

Handling Editor: N. Ravishankar.

Address correspondence to E-mail: quwenqing@buaa.edu.cn

<https://doi.org/10.1007/s10853-023-08372-z>

metals for brazing traditional ASS have been developed, such as Ni-based, Cu-based and Ag-based fillers [1, 2]. Due to low vapor pressure and low melting temperature, Ag–Cu-based alloy is most commonly used for vacuum brazing stainless steel. The brazed structures are often used below 400 °C.

However, poor wettability is an important issue in brazing stainless steel [3]. Stainless steel is covered by a very thin, tenacious oxide layer, which is a barrier for wetting and brazing by liquid metal [4]. In order to improve the wettability, several methods have been developed. High heating temperature can help obtain good wettability [5, 6]. But high temperature will damage the performance of the structure. High vacuum condition is helpful to obtain good wetting [7]. But high vacuum environment has high requirement for equipment, resulting in high cost. The addition of Mn and Zn is conducive to improve the wettability and fluidity of Ag–Cu alloy [1, 2, 8]. But zinc and manganese are not suitable for vacuum brazing due to high vapor pressure. In addition, the interaction between filler metal (FM) and SS and diffusion of filler components into SS can also improve the wettability [9, 10]. At present, nickel plating on stainless steel surface is a common method to improve wettability [1–3].

However, the necessity of nickel in brazing SS with AgCu alloy is still controversial. Sánchez [11] believed stainless steel should be nickel plated on surface to increase the wettability. Venkateswaran [12] proposed nickel coating could help achieve good wettability and minimize the intergranular penetration of filler metal into base metal when martensitic stainless steel (MSS) and AISI 321 ASS were brazed with CuAgMnZn filler. On the other hand, some reports claimed SS could obtain satisfactory brazing joints without nickel plating. Kumar [13] demonstrated hermetically sealed sound and strong copper-316L SS vacuum brazed joints were obtained without nickel electroplating. The only pretreatment requirement was simple ultrasonic cleaning of SS. Fukikoshi [14] reported satisfactory brazed joint of copper and electroless SS using Ag50Cu filler was obtained. Kozlova [15] proposed Ni had no measurable effect on wetting curve of Ag–Cu alloy on 321 steel. Therefore, the effects of nickel on the wettability and brazeability of stainless steel by Ag–Cu alloy need to be studied systematically.

Alloying elements were often added in filler to improve the wettability and joint performance. And, alloying elements often play a role by influencing the interface. Shi [16] reported the accumulation of Ni at Cu interface increased nanoindentation hardness, which caused the transformation of fracture location and the improvement of tensile strength during induction brazing of pure Cu and 304 SS with AgCuZnMnNi filler. Kang [7] reported oxygen added in Ag–Cu alloy could remove and modify the oxide layer on stainless steel surface to improve the wettability. Frage [17] reported small addition of Ni in Au could improve the wettability in Au/TiC system, which prevented the formation of graphite layer on TiC substrate by dissolution, as the solubility of C in molten Ni is several orders of magnitude higher than in Au.

Interfacial reaction and interfacial behavior are important in dissimilar materials joining. Interfacial reaction can modify the chemistry, structure of the contact area [18]. Interfacial reaction can improve wettability by forming new compound layer or removing wetting barrier (oxide film) on ceramic and metallic solids surface [18]. For example, the interfacial reaction phase TiO promotes the TiCu liquid wettability in TiCu/Al₂O₃ system [19]. Formation of intermetallic at interface, which is possible by diffusion of reacting components through the thin oxide layer, can disrupt the oxide layer and create a clean surface [20]. However, research about the influence of Ni on AgCu/SS interfacial reaction is still limited at present.

The wetting and brazing behaviors of stainless steel by Ag–Cu based alloy were studied in this paper. And tensile shear test was used to evaluate the joining performance. The purpose of this paper is to analyze the role of Ni in this process. As Ni is mainly enriched at solid–liquid interface, the focus of the test is to understand how nickel affects the physical and chemical interactions at FM/SS interface, such as the diffusion and dissolution of different elements and formation of phases at the interface. On this basis, the reasons for the improvements of filler wettability and joint strength after adding Ni in filler were studied. It is generally believed the wetting of stainless steel was caused by the removal of oxide film on surface [15, 21], so the effect of Ni on the removing of oxide film was also studied.

Materials and methods

The base metals (BM) used in this work were 304 SS with dimension of $20 \times 20 \times 1 \text{ mm}^3$ and high purity oxygen free electronic grade copper with dimension of $10 \times 20 \times 1 \text{ mm}^3$. Filler metals in form of foil with thickness of $100 \mu\text{m}$ were supplied by General Research Institute for Nonferrous Metals. Some steel plates were nickel plated with thickness of $7\text{--}10 \mu\text{m}$ [(Ni) SS]. The chemical composition of filler metals and base metal is shown in Table 1.

Wetting test and brazing test were carried out in a vacuum furnace. The vacuum level was maintained in the range of $5 \times 10^{-3} \text{ Pa}$ to $3 \times 10^{-3} \text{ Pa}$ during the heating and cooling process by using mechanical pump and oil diffusion pump. The substrates and filler metals were mechanical ground and cleaned in ethanol in an ultrasonic bath before the experiments.

Wetting experiment was performed by sessile drop method [22]. The filler metal ball with a weight of 0.2 g was placed in center of the steel plates. The wetting specimens were heated at the rate of $15 \text{ }^\circ\text{C}/\text{min}$ to $750 \text{ }^\circ\text{C}$ for 30 min and then heated to the holding temperature ($830 \text{ }^\circ\text{C}$, $850 \text{ }^\circ\text{C}$, $870 \text{ }^\circ\text{C}$ and $890 \text{ }^\circ\text{C}$) at the rate of $15 \text{ }^\circ\text{C}/\text{min}$. After holding 10 min, the samples were cooled to room temperature in the furnace. After taking out the sample, cut it through the center of the filler ball with wire cutting, measure the contact angle, and take the average value of at least three samples. Brazing experiment was carried out by placing filler metal foil between steel plate and copper plate. The brazing assembly was heated to $850 \text{ }^\circ\text{C}$ for 10 min. And then, furnace cooling to room temperature was followed using the same vacuum furnace as the wetting experiment. The heating process of brazing was also the same as that of the wetting experiment. Five different joints were brazed as shown in Table 2.

The interfacial microstructure and chemical composition were examined using optical microscope (OM, Axio Scope.A1, Germany) and scanning

electron microscope (SEM, Merlin Compact, Germany) equipped with an energy-dispersive X-ray spectrometer (EDS). The SEM analysis was operated using SE2 detector at a voltage of 15 kV with a work distance of 9.5 mm . Chemical composition profiles were determined by an electron probe microanalysis (EPMA). EPMA measurements were performed at an electron beam voltage of 15 kV by an EPMA microprobe (model; JXA 8230 microprobe, JEOL, Japan), and wavelength dispersive spectroscopy (WDS) was used for elemental mapping of the FM/SS interface.

The tensile shear strength of Cu/304 joints was measured using universal testing machine (SANS 5504) to estimate the mechanical properties. The cross-head moving speed was $0.5 \text{ mm}/\text{min}$. At least five specimens were used to determine the average strength of the brazed joints. The surface features of fracture specimens were examined with SEM. The schematic diagram of the single-lap specimen is presented in Fig. 1.

Results and discussion

Figure 2 shows the microstructures of AgCu-xNi fillers. At room temperature, the microstructure of AgCu-xNi filler is brown Cu solid solution (s,s) + white Ag solid solution + eutectic structure (shown by arrows). According to Ag-Cu-Ni ternary phase diagram [23], with the increase in temperature, the eutectic structure undergoes melting first, then the white Ag(s,s) melts, and finally, the brown Cu(s,s) melts. The AgCu-xNi filler is a single liquid phase at brazing temperature.

Wetting

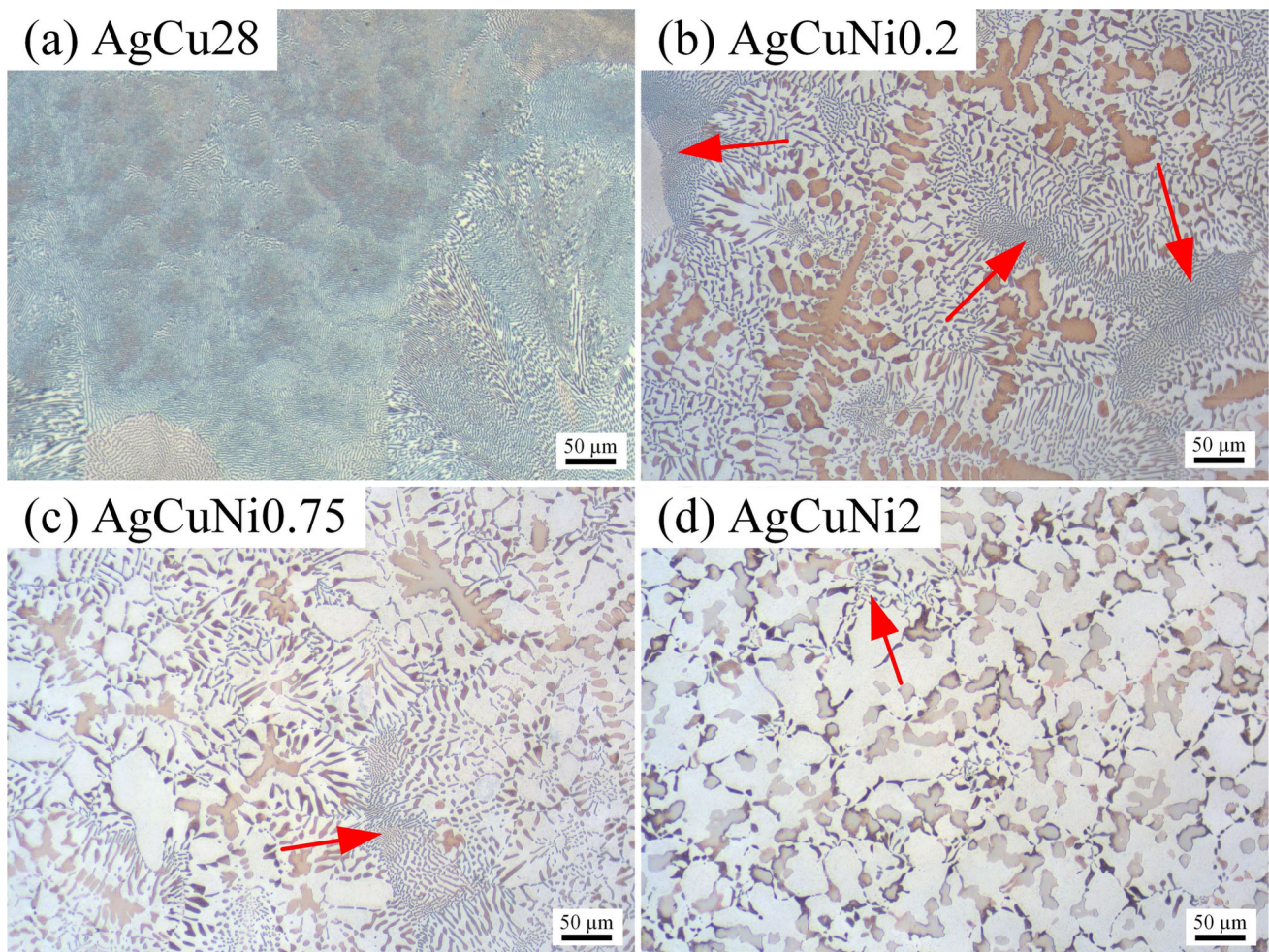
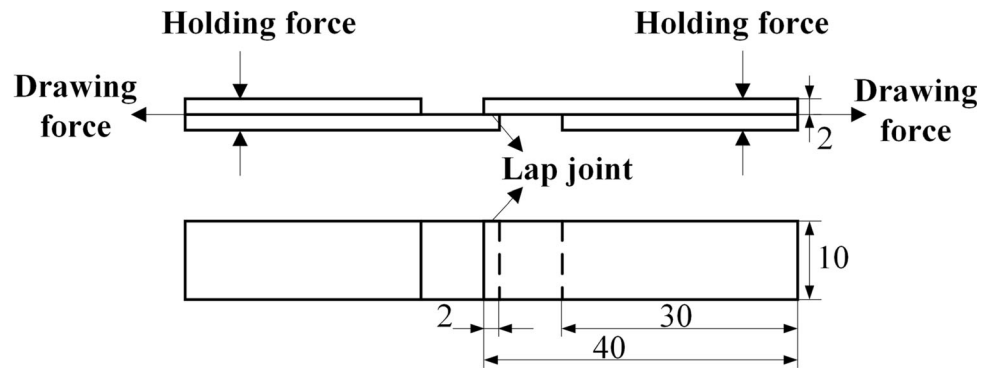
Figure 3 shows the variation of contact angle with Ni content in filler. The contact angle decreases with Ni content. At $830 \text{ }^\circ\text{C}$, the contact angle first decreases significantly and then decreases slowly. Because the

Table 1 Chemistry and solidification range of filler metals and base metal (wt%)

	Fe	Cr	Mn	C	Si	S	Ni	Ag	Cu	Melting range ($^\circ\text{C}$)
AgCu28	–	–	–	–	–	–	–	72	28	779
AgCuNi0.2	–	–	–	–	–	–	0.2	71.8	28	782–785
AgCuNi0.75	–	–	–	–	–	–	0.75	71.25	28	787–796
AgCuNi2	–	–	–	–	–	–	2	70.56	27.44	797–829
304 SS	Bal	18.20	0.28	0.04	0.59	0.003	9.13	–	–	1398–1454

Table 2 Five different joints

	Joint 1	Joint 2	Joint 3	Joint 4	Joint 5
BM 1	Copper	Copper	Copper	Copper	Copper
BM 2	SS	SS	SS	SS	(Ni) SS
FM	AgCu28	AgCuNi0.2	AgCuNi0.75	AgCuNi2	AgCu28

Figure 1 Schematic diagram of tensile shear test specimens.**Figure 2** Microstructures of AgCu-xNi fillers.

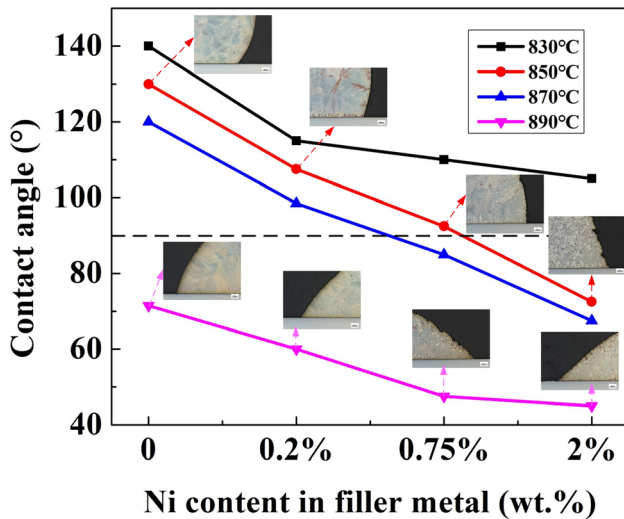


Figure 3 Variation with Ni content in contact angle on 304 SS substrates.

melting point of filler metal increases with Ni content, and the fluidity of filler metal becomes worse. The contact angle decreases linearly at 850 °C and 870 °C. The contact angle decreases slowly at 890 °C.

The wettability can be affected by wetting temperature. Figure 3 shows the contact angle decreases with wetting temperature. It is worth noting it decreases significantly at 890 °C. The contact angle of AgCu28 alloy at 830–870 °C is in the range 120°–140°, which are typical for noble metal/oxide couples [4]. And it is considered to be on oxidized steel. The contact angle of AgCu28 alloy at 890 °C close to 60°, which is metal/metal system [4]. McGurran and Ambrose [24] proposed SS could obtain good wetting by heating in high vacuum above a certain temperature. Kozlova [15] deduced that SS could be deoxidated by residual carbon through thermodynamic calculations, which was compatible with experimental findings. Zhuang [25] proposed small amount of carbon could deoxidate the oxide film, and the starting temperature was about 900 °C. It can be inferred the oxide film on stainless steel surface may have almost been reduced at 890 °C, leading to metal/metal contact.

The commonly used brazing temperature of AgCuNi filler is about 850 °C. Figure 4 shows the microstructures of four FM/SS interfaces at 850 °C, and the EDS results were shown in Table 3. A few small blocky Cu solid solution formed at AgCu28/SS interface. EDS line scans show the interdiffusion between AgCu28 and SS is weak. That is because Ag

and Fe are immiscible in solid and liquid state, and the mutual solubility of Cu and Fe is extremely limited. Kozlova [15] reported limited penetration of the liquid into steel grain boundary (GB) occurred at AgCu/SS interface during wetting experiments. The penetration depth depends on the steel, several microns for 321 steel and only a few hundred nm for 316L steel and 316Ti steel. But no obvious penetration of filler into 304 SS is observed in Fig. 4a, or maybe the penetration was very weak.

A Cu(s,s) layer formed at FM/SS interface after adding Ni in filler, Ni content in which was high (point 3, point 10). Figure 4b shows the AgCuNi0.2/SS interfacial microstructure. In point b, Fe content suddenly decreases, and Ag content is high. It indicates the filler may penetrate into steel. In point c, Fe content suddenly decreases, and a Cu peak appears. It indicates it may be Cu penetrating into steel GB firstly. Figure 4d shows the composition of point d is close to that of point e, indicating point d is a grain detached from the bulk. Figure 4c, d shows some steel grains separate from the substrate at AgCuNi0.75/SS interface and AgCuNi2/SS interface (red arrows).

Ni line scans show large amount of Ni concentrated near FM/SS interface, and the amount of Ni concentrated near interface increases with the increase of Ni content in filler. It indicates Ni in liquid filler is mainly enriched at solid–liquid interface at wetting temperature. Asl [26] found impurities in Ni–Bi liquid were discharged from the liquid and adsorbed at GB and solid–liquid interface. Mu [27] proposed Ni in AgCuNi liquid was mainly enriched at solid–liquid interface due to chemical potential gradient. Compositions of point 8 and point 9 show large amount of Ni have diffused into steel. From Cu(s,s) layer to steel, Ni content increases instantaneously. It indicates Ni has a strong tendency to diffuse into steel, because Ni and ASS are infinitely miscible.

Figure 5 shows the EPMA composition profile maps in AgCuNi0.2/SS interface at 850 °C. Fe map shows the topmost steel grains are exposed. Ag map shows some Ag atoms are segregated between the exposed steel grains. But Ag does not diffuse into steel, as Ag and Fe, Ag and Cr, Ag and Ni are all immiscible in solid and liquid state. Figure 5b shows Cu mainly diffuses into steel along GBs.

Grain boundary penetration of molten Cu into steel is a common issue when Cu/Cu-based alloy and steel

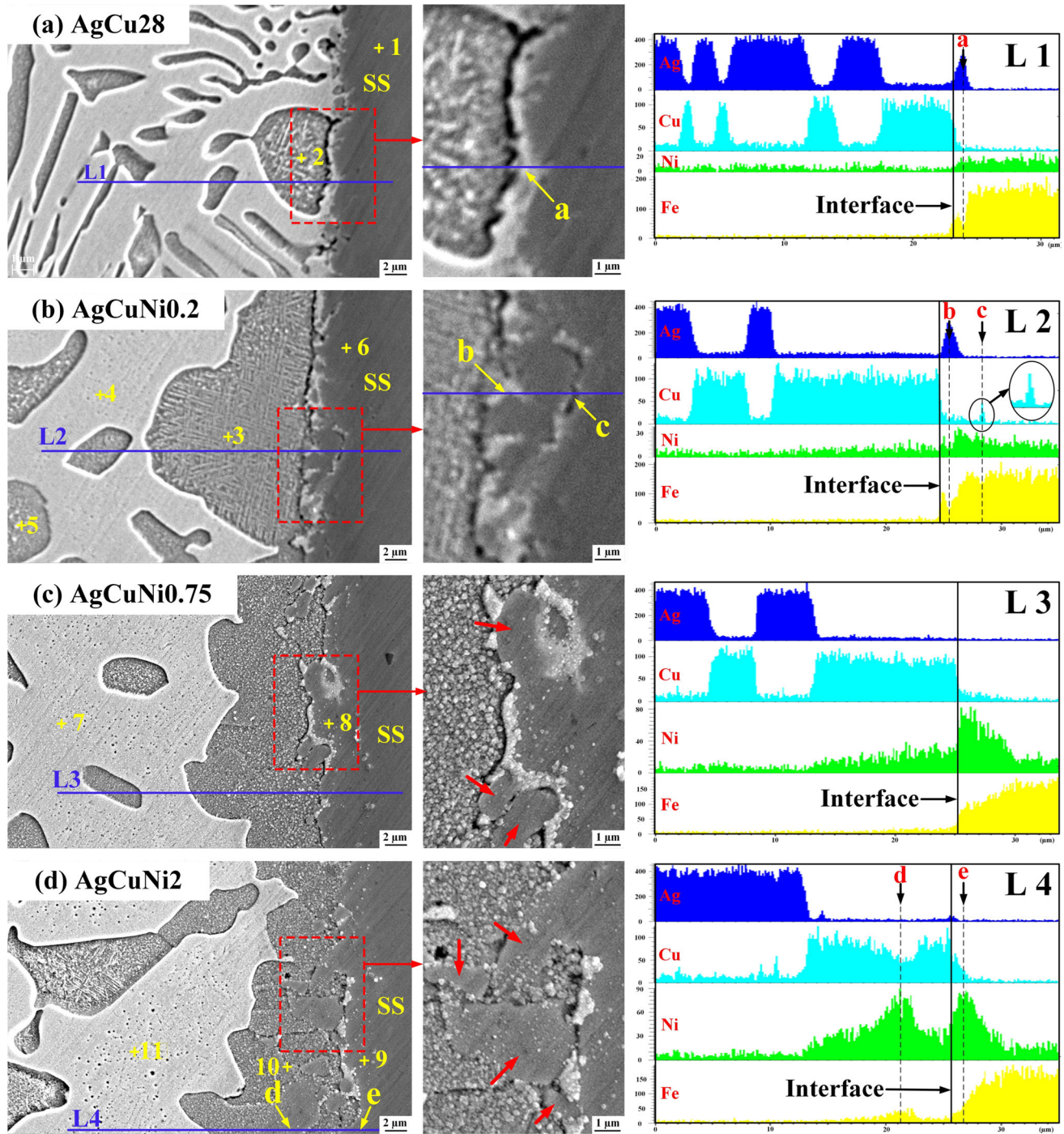


Figure 4 Interfacial microstructures of **a** AgCu28/SS interface, **b** AgCuNi0.2/SS interface, **c** AgCuNi0.75/SS interface, **d** AgCuNi2/SS interface after wetting test at 850 °C.

are welded, which is known as the phenomenon of Cu-induced hot cracking in steels [28–33]. When stainless steel is brazed or welded by some Cu-containing filler metals, molten filler metal can also penetrate into steel GBs. Sun [34] and Silze [35] found

during wetting of pure copper on 304 SS/304L SS, liquid copper penetrated into the substrate along GB, leading to the separation of steel grains at the interface. Silze [36] found during wetting of CuGa alloy on 304L SS, the liquid penetrated along GBs of the

Table 3 EDS results from Fig. 4 (wt%)

Points	Ag	Cu	Ni	Fe	Cr	Mn	Phases
1	0.16	0.33	9.07	71.28	18.79	0.37	SS
2	22.84	76.09	0.23	0.68	0.16	0	Cu(s,s)
3	7.63	86.85	3.78	1.57	0.16	0.01	Cu(s,s)
4	94.43	5.97	0	0	0	0	Ag(s,s)
5	7.98	91.44	0.39	0.21	0.09	0	Cu(s,s)
6	0.11	2.42	10.03	68.49	17.78	1.17	SS
7	92.34	7.15	0.30	0	0.07	0.14	Ag(s,s)
8	7.16	19.09	41.44	27.06	4.90	0.35	(Ni, Fe, Cu) (s,s)
9	0.27	18.99	44.94	28.70	6.94	0.16	(Ni, Fe, Cu) (s,s)
10	0.52	72.55	21.32	4.65	0.90	0.06	(α -Cu, Ni)
11	89.00	10.60	0	0.15	0.20	0.11	Ag(s,s)

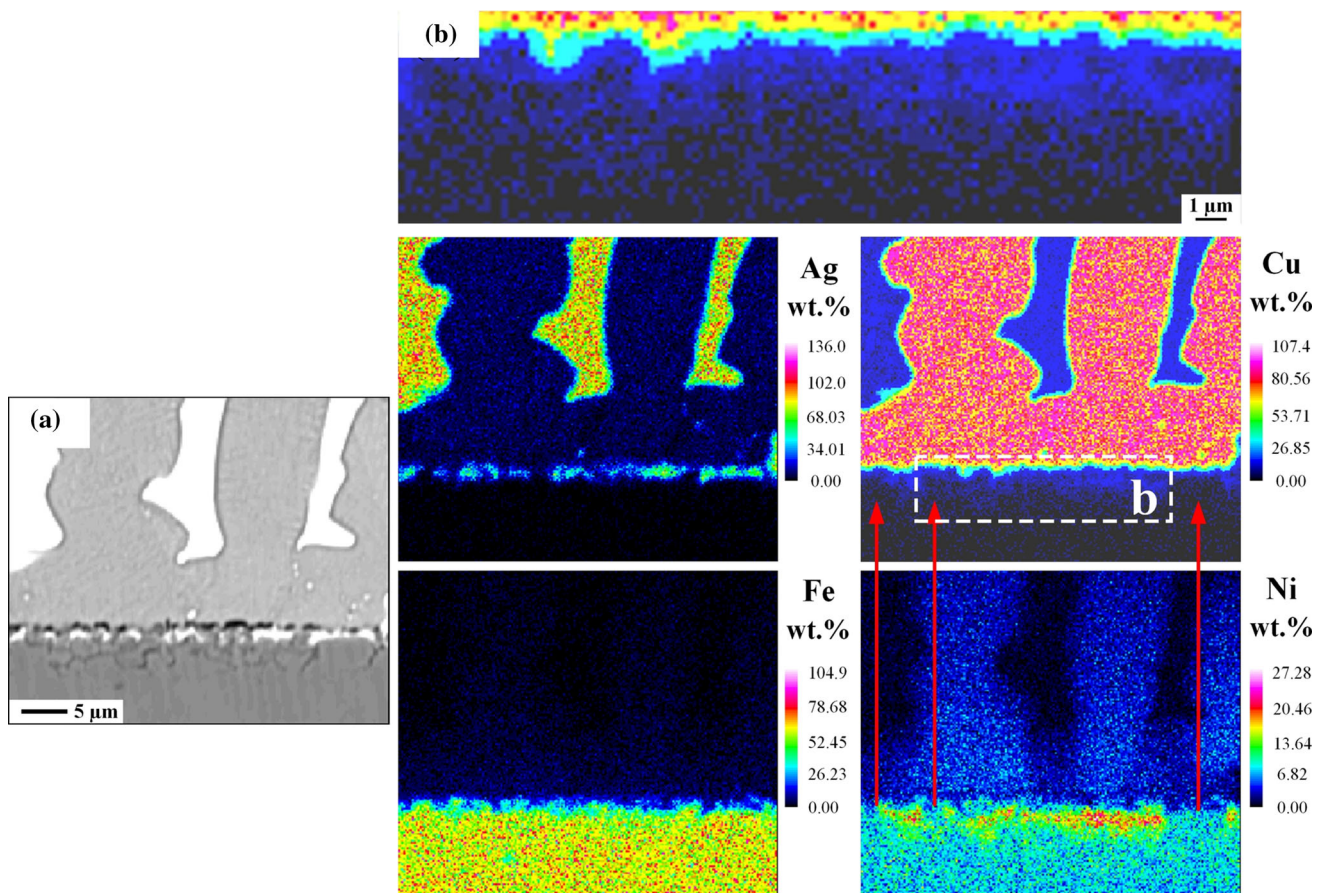


Figure 5 EPMA composition profile maps of Ag, Cu, Fe and Ni in AgCuNi0.2/SS wetting interface at 850 °C.

substrate. He believed high Cu content in liquid caused this behavior, and Cu first penetrated into steel. Venkateswaran [12] found CuAgMnZn filler penetrated into GB of ASS. Chen [37] proposed Cu penetrating cracks appeared in heat-affected zone (HAZ) of arc-brazing 316L/316LN stainless steel joints with CuSi3, CuSi3Mn, Ag45CuSnNi fillers. He believed Cu content in filler had an important effect

on the formation of Cu penetrating cracks. Lee [38] proposed cracks were detected in HAZ of stainless steel, and Cu peak was detected in the crack opening area during gas tungsten arc welding of ASS and Al brass with CuAl, CuSn, NiCu fillers. The reason for the penetration of molten Cu into steel GB is still unclear [29, 30, 39–41]. This paper will not study this. We should know that liquid copper and some Cu-

containing filler can penetrate into steel GB, and Cu in liquid first penetrates into steel GB. Cu content in liquid filler has an important effect on the penetration, and high Cu content in liquid can cause this behavior. AgCu28 liquid filler does not penetrate into steel GB, indicating the Cu content in liquid is too low to penetrate ($\omega_{\text{Cu}} = 28 \text{ wt\%}$). Grain boundary penetration occurs after adding Ni in filler. It can be inferred Cu content in liquid near the interface may increase after adding Ni ($\omega_{\text{Cu}} > 28 \text{ wt\%}$). The reason for that will be discussed later.

Ni map shows the diffusion layer of Ni into steel is discontinuous, which only occurs in the area where Cu has diffused into. Because the oxide layer on stainless steel surface hinders the Ni diffusion into steel, but Ni can diffuse into steel interior along the Cu-penetrated steel GB. Once Ni passes through the oxide layer, Ni will diffuse into grains on both sides of GB. Then, Cu can diffuse into the grains, as Cu and Ni are infinitely miscible. So, it can be seen that Cu not only diffuses along GBs, but also diffuses into steel grains. It is not completely same as the penetration of Cu-containing filler into steel mainly along GBs in references [34–38]. After Cu and Ni in liquid near the interface diffused into steel, Ag in liquid was left near the interface.

Figure 6 shows the EPMA composition profile maps in AgCuNi2/SS interface at 850 °C. Fe map shows some steel grains separated from the bulk and large amount of Fe dissolved in liquid filler. Ni map shows Ni content in steel surface and the separated steel grains is very high (about 46.11 wt% or higher). The diffusion layer of Ni into the fresh metal surface continues (black dotted line), as Ni can directly diffuse into steel after topmost steel grains detach from the bulk. Cu map shows large amount of Cu have diffused into steel. Compared with AgCu28/SS interface, the interdiffusion between filler and SS is enhanced after adding Ni.

Figure 7 is the schematic diagram of AgCu-xNi/SS interfacial reaction at 850 °C. AgCu-xNi filler has been melted into liquid completely at 850 °C (Fig. 7a). As the linear expansion coefficient between the metal and oxide film is different [42], the oxide film cracks during heating up [34]. Silze [36] found liquid Cu preferentially spreads laterally along steel GB before covering the whole grain, indicating the oxide film cracks along GBs. The dissolution of Fe can also break the bond between oxide film and substrate [34]. The composition of liquid filler is not uniformly

distributed at 850 °C. A large number of Ni in liquid is enriched at solid-liquid interface (Fig. 7b). But the oxide film hinders the Ni diffusion into steel. Pique [43] proposed Cu was strongly adsorbed at liquid Ag/solid Fe interface. The enrichment of Ni at solid-liquid interface leads to the increase of Cu content in liquid near solid-liquid interface [44], we call it Cu-rich liquid ($\omega_{\text{Cu}} > 28 \text{ wt\%}$) (Fig. 7c). That causes the penetration of liquid filler into stainless steel. Fe can dissolve in Cu-rich liquid with high Ni content, as Fe and Ni are infinitely miscible. Cu in Cu-rich liquid penetrates into steel GB through the cracks on oxide film (Fig. 7d) [34]. Then, Ni diffuses into steel along the penetrated GB (Fig. 7e). The topmost steel grains gradually separate from the bulk, exposing the metal surface without oxide film (Fig. 7f). Then, Ni can directly diffuse into steel after the oxide film is removed. Ni content at solid-liquid interface gradually decreases. Cu-rich liquid formed near solid-liquid interface gradually decreases. Grain boundary penetration gradually stops.

Kozlova [15] proposed the wetting of AgCu alloy on stainless steels can be divided into two stages: (1) spreading is controlled by steel deoxidation and leads to a reduction in the contact angle; (2) dissolution leads to a further reduction in contact angle. The wetting interfaces at 890 °C were studied to analyze dissolutive wetting in the second stage after the oxide film was removed.

Figure 8a shows the microstructure of AgCu28/SS interface at 890 °C, and the EDS results were shown in Table 4. Fe content in blocky Cu(s,s) at interface is 1.58 wt% (point 12), but the blocky Cu(s,s) formed at interface is few. Ag, Cu contents in steel surface are low (point 14). Therefore, the interdiffusion between AgCu28 and SS is still limited at 890 °C. Figure 8b shows the microstructure of AgCuNi0.2/SS interface at 890 °C, and the EDS results were shown in Table 4. Compared with AgCu28/SS interface (Fig. 8e), the metallurgical bonding between AgCuNi0.2 and SS is tighter (Fig. 8f), and the amount of blocky Cu(s,s) formed at interface increases. Compared with AgCuNi0.2/SS interface at 850 °C, grain boundary penetration did not occur, no continuous Cu(s,s) layer formed at interface, Ni content in Cu(s,s) decreased (point 15 vs point 3), and the filler was closer to eutectic structure. These indicate most Ni at solid-liquid interface has diffused into steel.

Figure 9 shows EPMA composition profile maps in AgCuNi2/SS interface at 890 °C. Ni map shows the

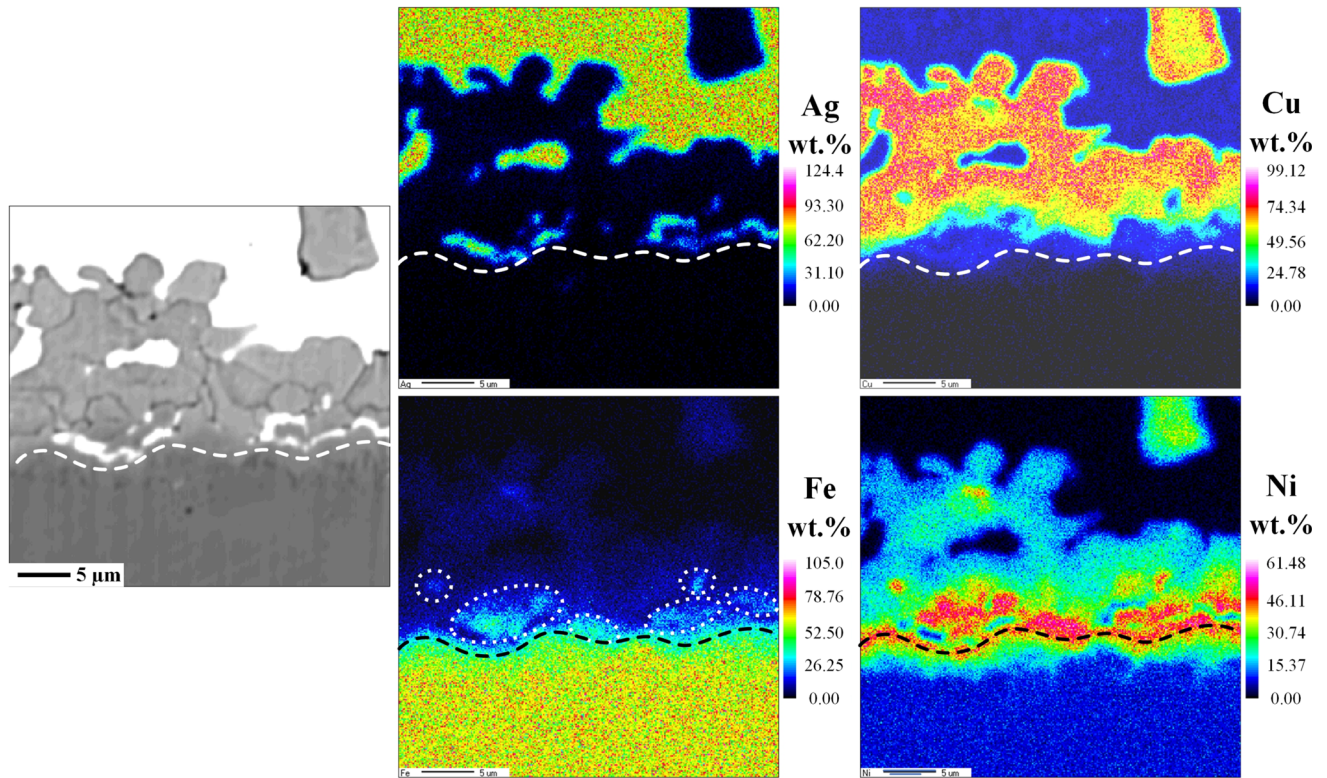
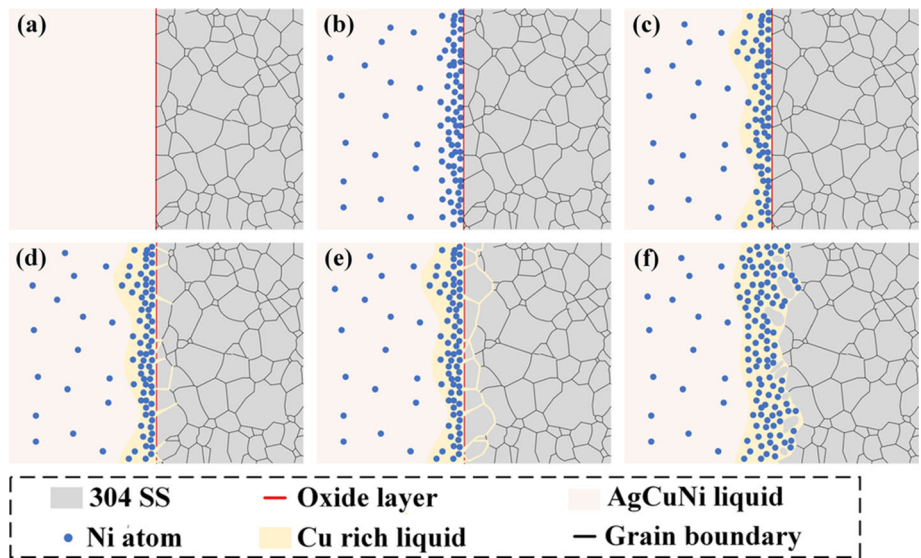


Figure 6 EPMA composition profile maps of Ag, Cu, Fe and Ni in AgCuNi₂/SS wetting interface at 850 °C.

Figure 7 Schematic diagram of AgCu-xNi/SS interfacial reaction at 850 °C.



diffusion layer of Ni into steel is flat, continuous and uniform, as Ni at the interface can directly diffuse into steel after oxide film is deoxidized. Ni content in Cu(s,s) layer at interface is lower than that in AgCuNi₂/SS interface at 850 °C, as more Ni have diffused into steel. Figure 8c, d show the microstructures of AgCuNi_{0.75}/SS interface and

AgCuNi₂/SS interface at 890 [Error hu2103], respectively. And the magnifications of Fig. 8g, h shows (γ-Fe, Ni) layer in light color with a thickness of about 4 μm formed on steel surface (point 20). The amount of grain detached from the substrate is less than that at 850 °C (red arrows). That is because Cu-rich liquid formed at solid-liquid interface is less,

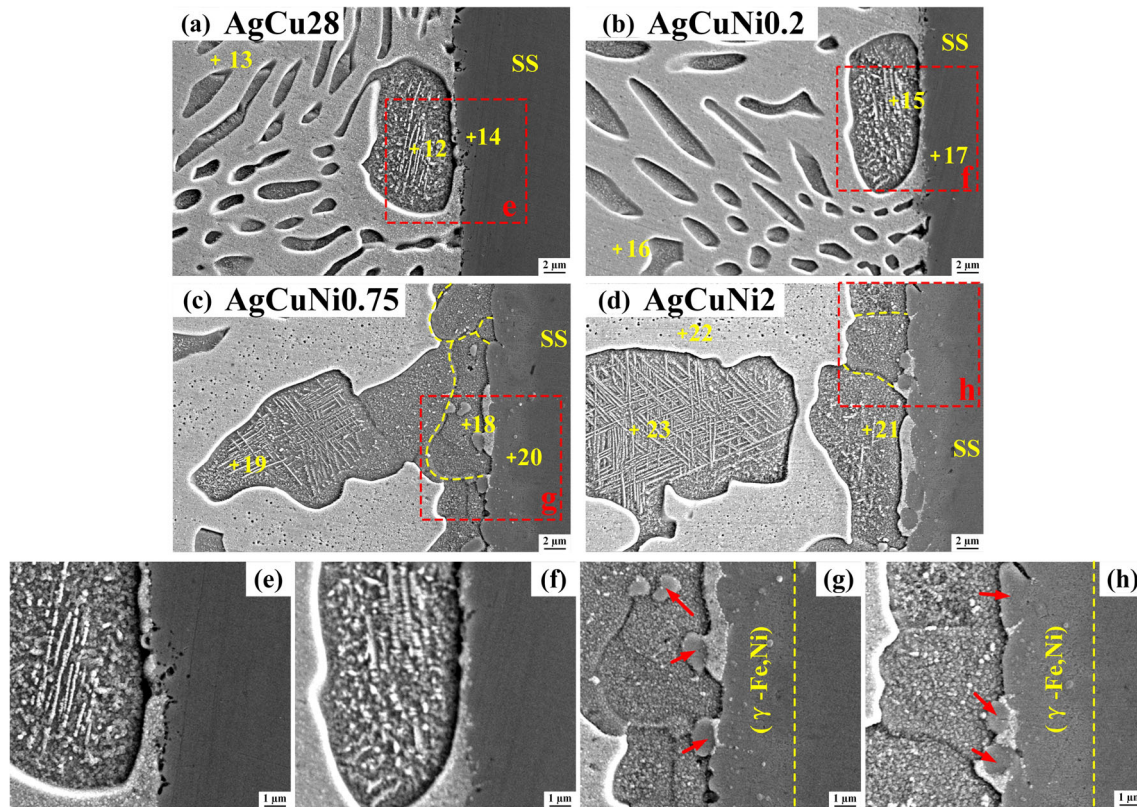


Figure 8 Interfacial microstructures of **a** AgCu28/SS interface, **b** AgCuNi0.2/SS interface, **c** AgCuNi0.75/SS interface, **d** AgCuNi2/SS interface after wetting test at 890 °C,

e magnification of the AgCu28/SS interface, **f** magnification of the AgCuNi0.2/SS interface, **g** magnification of the AgCuNi0.75/SS interface, **h** magnification of the AgCuNi2/SS interface.

and grain boundary penetration is weak at 890 °C. (α -Cu, Ni) containing a lot of Fe formed at the interface (yellow dotted line, point 18). Cu map shows large amount of Cu have diffused into steel (Cu content in steel surface is more than 10 wt%). That is because Cu in liquid can diffuse into (γ -Fe, Ni). Thus, the interdiffusion between FM and SS is enhanced after adding Ni at 890 °C, resulting in a further reduction in contact angle.

Brazing

Mechanical property of joints

Figure 10 shows the tensile shear strength of five different joints. The joint strength increases with the increase of the added Ni amount. The strength of Cu/AgCu28/SS joint is the lowest (138.68 MPa). The strength of Cu/AgCu28/(Ni)SS joint is the highest (194.78 MPa), which is 40.45% higher than that of Cu/AgCu28/SS joint.

Figure 11 shows the macroscopic morphologies (upper side) and cross section at SS side (lower side) of fracture. Cu/AgCu28/SS joint fractured on FM/SS interface. It indicates FM/SS interface is the weakest location of the joint in the absence of Ni. The Cu/AgCuNi0.2/SS, Cu/AgCuNi0.75/SS and Cu/AgCuNi2/SS joints fractured on FM/SS interface and Cu base metal. The Cu/AgCu28/(Ni)SS joint fractured on Cu substrate. With the increase of the added Ni amount, the fracture location transformed from FM/SS interface to Cu substrate, indicating the strength of FM/SS interface was enhanced after adding Ni.

Figure 12 shows the microscopic fracture morphologies of different joints. The fracture surfaces of Cu/AgCu28/SS joint and Cu/AgCuNi0.2/SS joint show the fracture mode of ductile–brittle mixture, with river-like patterns and small amounts of elongated dimples (Fig. 12a, b). The fracture surface of Cu/AgCu28/(Ni) joint shows obvious plastic fracture characteristics with a large number of dimples

Table 4 EDS results from Fig. 8 (wt%)

Points	Ag	Cu	Ni	Fe	Cr	Mn	Phases
12	8.49	89.32	0.26	1.58	0.42	0	Cu(s,s)
13	94.32	5.73	0	0.05	0	0.05	Ag(s,s)
14	0.19	0.30	8.51	71.40	18.20	1.41	SS
15	17.48	80.30	0.59	1.30	0.24	0.09	Cu(s,s)
16	94.38	5.12	0.17	0.07	0.12	0.15	Ag(s,s)
17	0.09	0.57	13.19	69.09	16.17	0.89	SS
18	2.08	78.11	14.88	4.12	0.64	0.17	(α -Cu, Ni)
19	10.65	88.17	1.41	0	0	0	Cu (s,s)
20	0.38	10.09	39.38	40.40	9.28	0.47	(γ -Fe, Ni)
21	6.18	83.34	8.97	1.24	0.11	0.16	Cu(s,s)
22	93.27	6.56	0	0.23	0	0.06	Ag(s,s)
23	6.55	86.74	6.22	0.28	0.16	0.04	Cu(s,s)

(Fig. 12c). The yield strength of AgCu28 alloy is 180 MPa [45]. In addition to the alloying effect of Ni and the supporting effect of BM on the seam, the yield strength of the brazing seam should be higher than 180 MPa. The strengths of Cu/AgCu28/SS joint and Cu/AgCuNi0.2/SS joint were lower than 180 MPa, because fracture occurred on FM/SS interface and had brittle fracture characteristics.

Therefore, the FM/SS interface bonding seriously affects the joint strength.

Microstructures of joints

Cu/AgCu28/SS joint, Cu/AgCuNi0.2/SS joint, Cu/AgCuNi0.75/SS joint, Cu/AgCuNi2/SS joint and Cu/AgCu28/(Ni) SS joint were brazed. Sound joints were achieved without pores and cracks. Figure 13 shows the microstructures of FM/SS interface in different joints. In Cu/AgCu28/SS joint, no Cu(s,s) formed at FM/SS interface. Cu(s,s) formed at FM/SS interface in other four joints after adding Ni. The amount of Cu(s,s) formed increases with the increase of the added Ni amount. Line scanning results show the interdiffusion between FM and SS increases with the increase of the added Ni amount. The formation of Cu(s,s) at FM/SS interface and the enhancement of interdiffusion between FM and SS strengthen the FM/SS interface, leading to the increase in joint strength after adding Ni.

In wetting experiment, the volume of filler ball is large (0.2 g in weight), the total amount of Ni in filler ball is large, the solid–liquid interface area is small ($\pi r^2 = 12.56 \text{ mm}^2$), and the amount of Ni enriched at

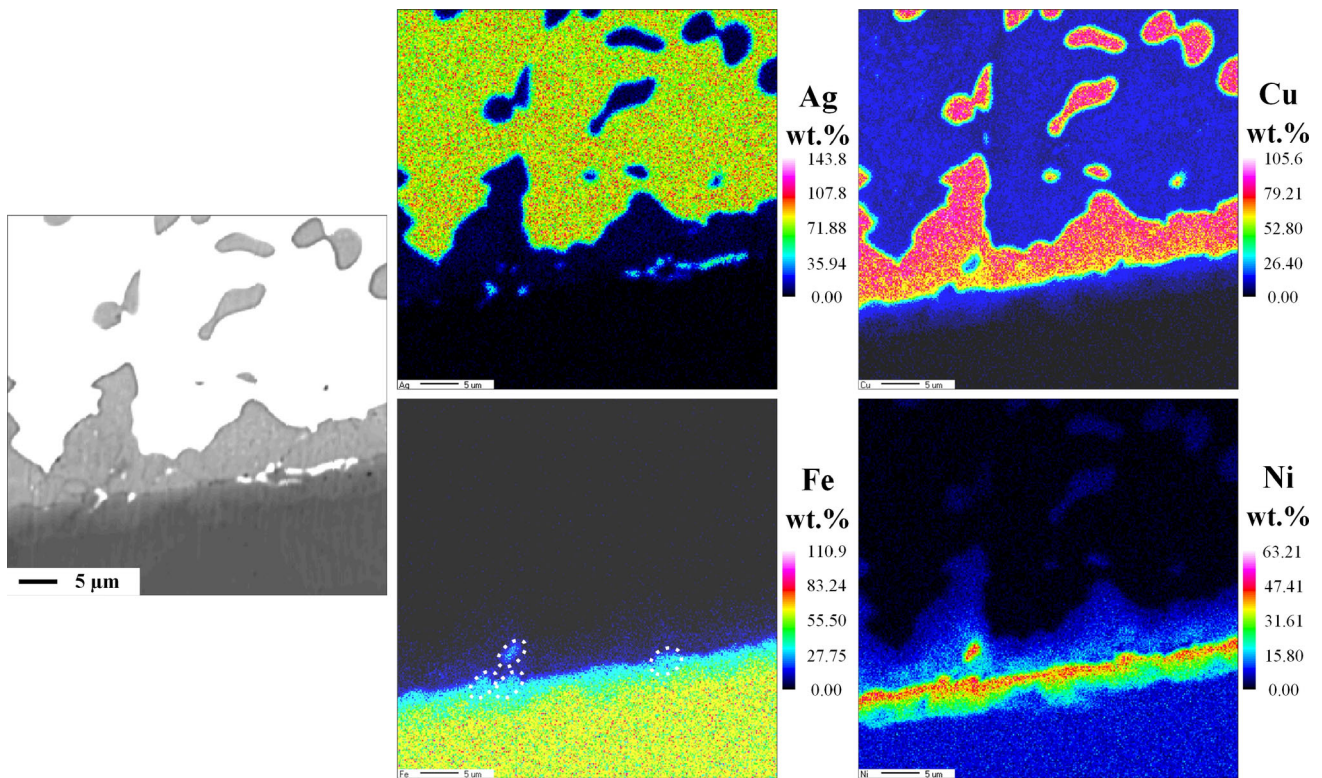


Figure 9 EPMA composition profile maps of Ag, Cu, Fe and Ni in AgCuNi2/SS wetting interface at 890 °C.

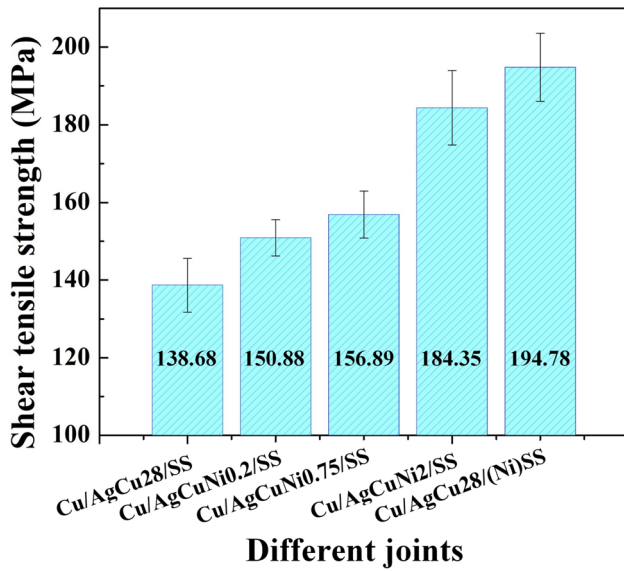


Figure 10 Tensile shear strength of different joints.

solid–liquid interface is large. In brazing experiment, the filler metal foil is thin (0.1 mm in thickness), the total amount of Ni in filler foil is small, the solid–liquid interface area is large ($2 \times 10 \times 20 = 400 \text{ mm}^2$), and the amount of Ni enriched at solid–liquid interface is small. Compared with wetting experiment, Ni concentration at the solid–liquid interface is relatively low, resulting in less Cu-rich liquid formed near the interface. The penetration of liquid filler into steel is weak, and the mutual diffusion between filler and stainless steel is less.

Conclusions

In this paper, wetting test and brazing test of 304 SS by Ag–Cu based alloy were performed under high vacuum conditions. The effect of Ni on the FM/SS

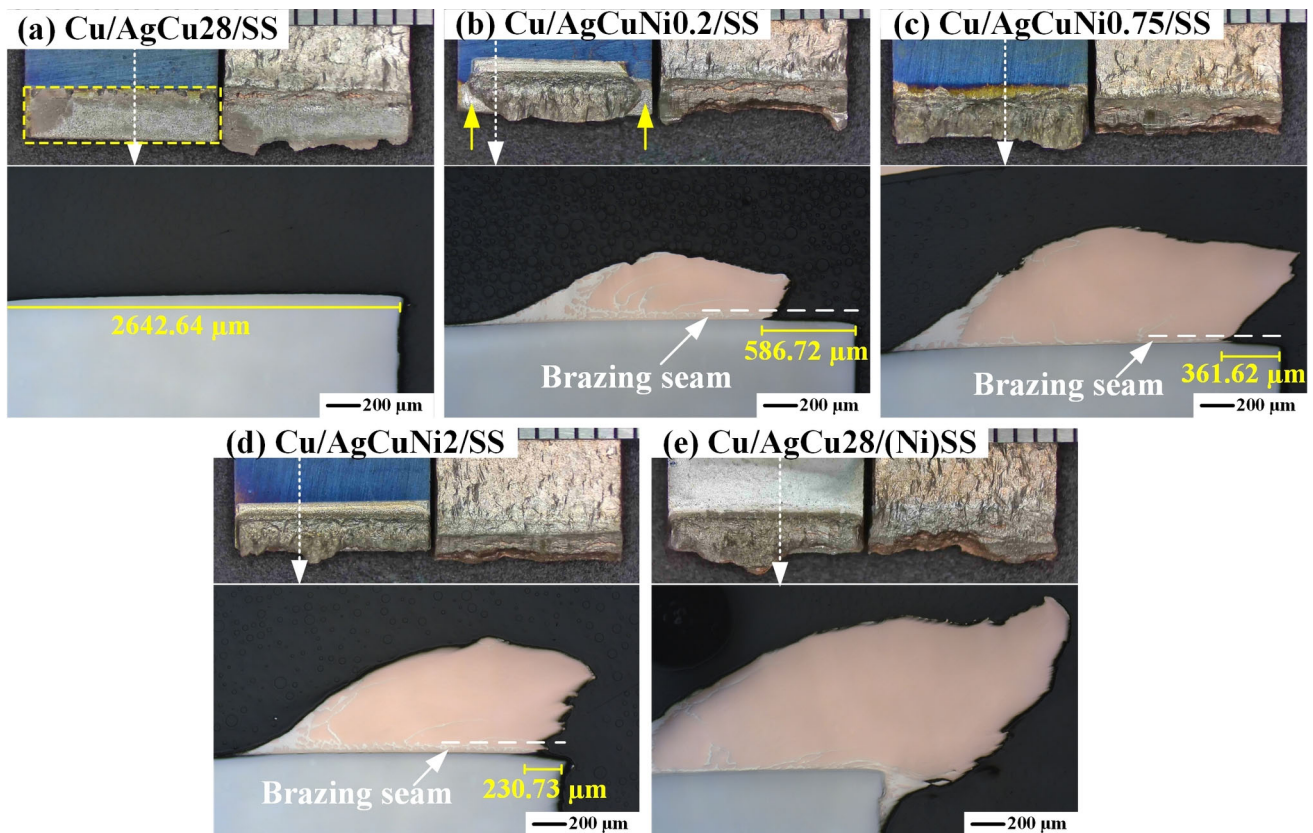
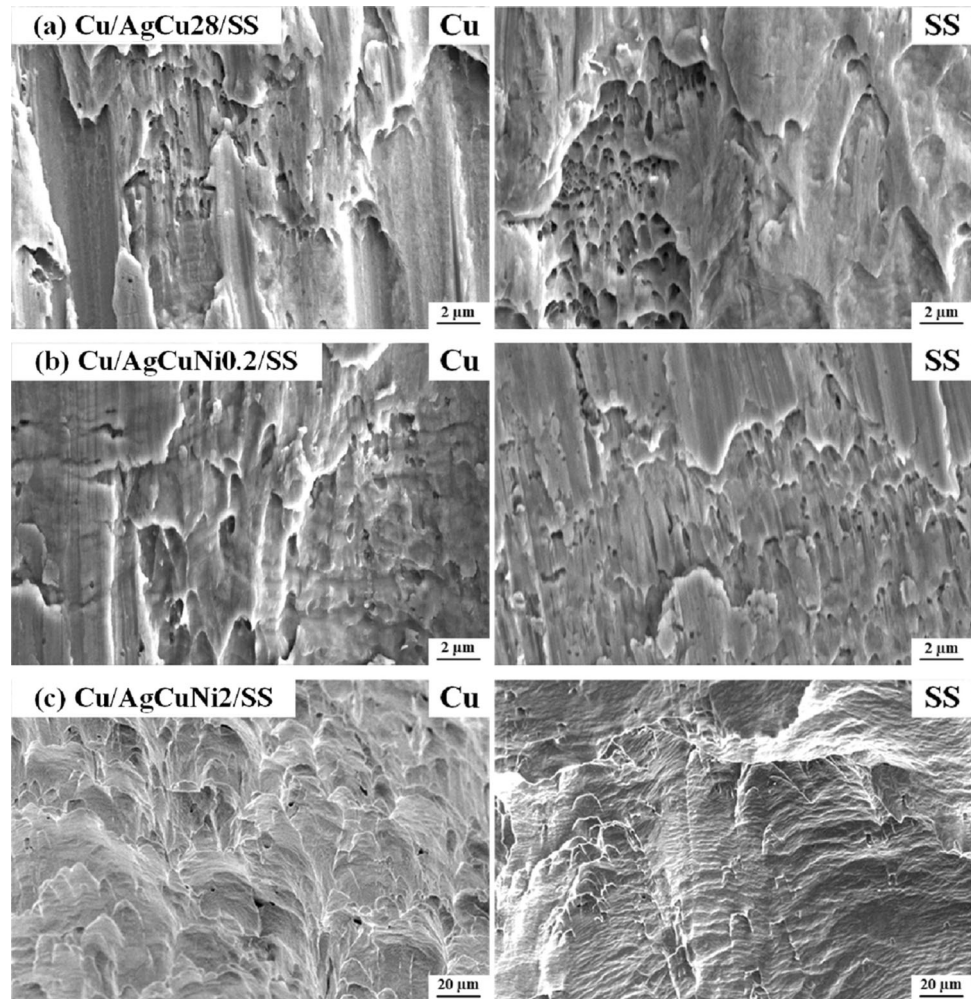


Figure 11 Macroscopic morphology (upper side) and cross section at SS side (lower side) of fracture (cut along the white dotted line) in **a** Cu/AgCu28/SS joint, **b** Cu/AgCuNi0.2/SS joint, **c** Cu/AgCuNi0.75/SS joint, **d** Cu/AgCuNi2/SS joint, **e** Cu/AgCu28/(Ni) SS joint.

Figure 12 Microscopic fracture morphologies in **a** Cu/AgCu28/SS joint, **b** Cu/AgCuNi0.2/SS joint, **c** Cu/AgCu28/(Ni) SS joint.



interfacial behavior was investigated by various techniques such as SEM, EDS, EPMA. The effects of interfacial reaction on filler wettability and joint strength were analyzed. The most important results can be summarized as follows:

- (1) The contact angle of Ag–Cu-based alloy on 304 SS substrate decreases and the strength of Cu/304 SS brazed joint increases with Ni content in filler metal. The strength of Cu/AgCu28/SS joint is 138.68 MPa, and the strength of Cu/AgCu28/(Ni)SS joint is 194.78 MPa, increased by 40.45%.
- (2) SEM and EPMA results show the filler penetrates into stainless steel and the topmost steel grains separate from the substrate, exposing the metal surface without oxide film after adding

- Ni in filler, which leads to the reduction in contact angle. At wetting temperature, a large amount of Ni in liquid enriched at solid–liquid interface, resulting in the increase of Cu content in liquid near the interface to form Cu-rich liquid, which caused the penetration of liquid filler. EDS and EPMA results show Cu first penetrates into steel grain boundary, which provides a path for Ni diffusion into stainless steel.
- (3) EPMA results show the interdiffusion between FM and SS is enhanced after adding Ni in filler, which leads to further reduction in contact angle. After the oxide film was removed, a large number of Ni directly diffused into stainless steel to form (γ -Fe, Ni) layer on stainless steel surface. Cu in liquid can directly diffuse into (γ -

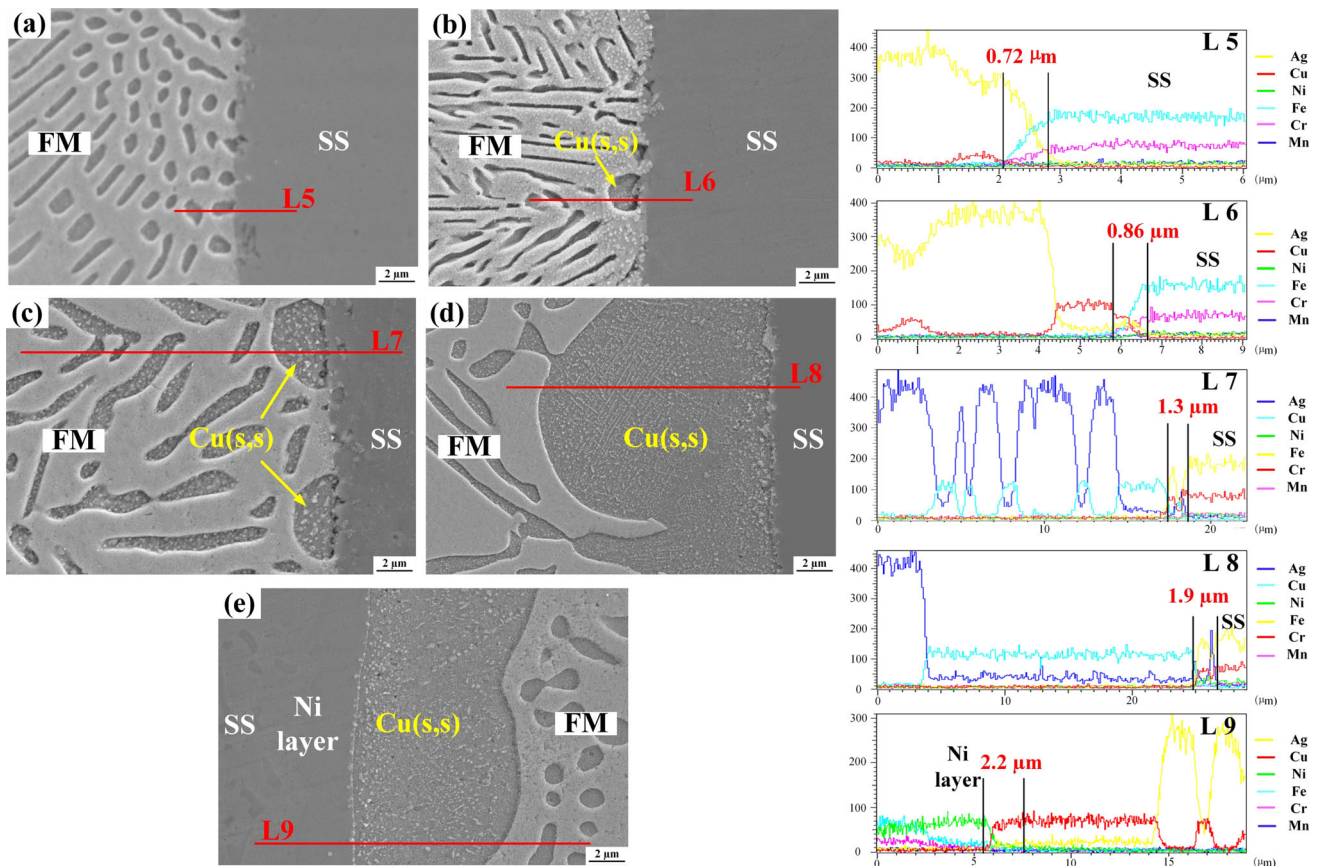


Figure 13 Microstructures of FM/SS interface in **a** Cu/AgCu28/SS joint, **b** Cu/AgCuNi0.2/SS joint, **c** Cu/AgCuNi0.75/SS joint, **d** Cu/AgCuNi2/SS joint, **e** Cu/AgCu28/(Ni) SS joint after brazing test at 850 °C.

Fe, Ni), not only along grain boundaries. Stainless steel can dissolve in Cu-rich liquid with high Ni content at solid–liquid interface.

- (4) In the absence of Ni, FM/SS interface is the weakest location of the joint. After adding Ni in filler, the rupture location transformed from FM/SS interface to Cu substrate, and the fracture mode changed from ductile–brittle mixed fracture to ductile fracture. The formation of Cu(s,s) at FM/SS interface and the enhancement of interdiffusion between FM and SS strengthen the FM/SS interface, leading to the increase in joint strength.

Acknowledgement

This work was supported by the key special projects of the national key R&D program [Grant No. 2017YFB0305700]. The authors of this paper sincerely

thank the teachers of the testing center of the school of materials science and engineering in Beihang university for their help.

Data availability

The raw/processed data required to reproduce the findings in this manuscript cannot be shared at this time as the data also form part of an ongoing study.

Declarations

Conflict of interest The authors declare that they have no conflict of interest in the work reported in this paper.

References

- [1] Jacobson DM, Humpston G (2005) Principles of Brazing. Asm International, pp 18–19

- [2] Schwartz MM (2003) *Brazing*, 2nd edn. ASM International, pp 50–56
- [3] Eustathopoulos N, Hodaj F, Kozlova O (2013) The wetting process in brazing. In: Sekulić DP (ed) *Advances in Brazing*. Woodhead Publishing Limited, Sawston, pp 8–10
- [4] Eustathopoulos N, Nicholas M, Drevet B (1999) *Wettability at high temperatures* (Pergamon materials series book 3). Pergamon, Oxford, pp 14–15
- [5] Committee on Brazing and Soldering (1976) *Brazing manual*, 3rd edn. American Welding Society, Miami, pp 24–27
- [6] Arata Y, Ohmori A, Cai HF (1983) Studies on vacuum brazing (Report II): removal of oxide film from stainless steel surface and brazing alloy spreading mechanism. *Trans JWRI* 12:27–34
- [7] Kang Y, Han J, Kim H, Lee J (2016) Effect of oxygen on the wettability of 304L stainless steel by liquid Ag–Cu eutectic alloy. *J Mater Sci* 51:1713–1721. <https://doi.org/10.1007/s10853-015-9511-1>
- [8] Lasko SV, Lasko NF (1988), *Soldering metals*. In: *Engineering*, ISBN 5-217-00268-9, 4th edn, Moscow, Russian, pp 23–26
- [9] Wall AJ, Milner DR (1961) Wetting and spreading phenomena in a vacuum. *J Inst Metal* 90:394–402
- [10] Okamoto I, Ohmori A, Arata Y, Chen D, Xu ZZ, Wu L (1980) A study on tunneling flow of filler metal in aluminum brazing. *Trans JWRI* 9:143–150
- [11] Sanchez L, Carrillo D, Rodriguez E, Aragon F, Sotelo J, Toral F (2011) Development of high precision joints in particle accelerator components performed by vacuum brazing. *J Mater Process Technol* 211:1379–1385
- [12] Venkateswaran T, Xavier V, Sivakumar D, Pant B, Ram GDJ (2017) Brazing of stainless steels using Cu–Ag–Mn–Zn braze filler: studies on wettability, mechanical properties, and microstructural aspects. *Mater Design* 121:213–228
- [13] Kumar A, Ganesh P, Kaul R, Yadav DP, Karnewar AK, Yedle KN, Gupta RK, Singh MK, Sankar PR, Bhatnagar VK, Sridhar R, Joshi SC, Kukreja LM (2016) Study on requirement of nickel electroplating in OFE copper-316L stainless steel brazed joints. *Int J Adv Manuf Technol* 87:2639–2651
- [14] Fukikoshi T, Watanabe Y, Miyazawa F, Kanasaki F (2014) Brazing of copper to stainless steel with a low-silver-content brazing filler metal. *IOP Conf Ser Mater Sci Eng* 61:012016
- [15] Kozlova O, Voytovych R, Devismes M-F, Eustathopoulos N (2008) Wetting and brazing of stainless steels by copper–silver eutectic. *Mater Sci Eng A* 495:96–101
- [16] Shi X, Li YX, Bai YJ, Zheng XB, Yao SY, Zhu ZT, Chen H (2021) Effect of Ni in pure Cu/304 stainless steel induction brazing joints. *Mater Charact* 182:111562
- [17] Frage N, Froumin N, Dariel MP (2002) Wetting of TiC by non-reactive liquid metals. *Acta Mater* 50:237–245
- [18] Dezellus O, Eustathopoulos N (2010) Fundamental issues of reactive wetting by liquid metals. *J Mater Sci* 45:4256–4264. <https://doi.org/10.1007/s10853-009-4128-x>
- [19] Kritsalis P, Coudurier L, Eustathopoulos N (1991) Contribution to the study of reactive wetting in the CuTi/Al2O3 system. *J Mater Sci* 26:3400–3408. <https://doi.org/10.1007/BF01124693>
- [20] Protsenko P, Terlain A, Traskine V, Eustathopoulos N (2001) The role of intermetallics in wetting in metallic systems. *Scripta Mater* 45:1439–1445
- [21] Keller DL, McDonald MM, Heiple CR, Johns WL, Hofmann WE (1990) Wettability of brazing filler metals. *Welding J* 69:31–34
- [22] Eustathopoulos N, Sobczak N, Passerone A, Nogi K (2005) Measurement of contact angle and work of adhesion at high temperature. *J Mater Sci* 40:2271–2280. <https://doi.org/10.1007/s10853-005-1945-4>
- [23] Liu XJ, Gao F, Wang CP, Ishida K (2008) Thermodynamic assessments of the Ag–Ni binary and Ag–Cu–Ni ternary systems. *J Electron Mater* 37:210–217
- [24] Ambrose JC, Nicholas MG (1996) Wetting and spreading of nickel-phosphorus brazes: detailed real time observations of spreading on iron-chromium substrates. *Mater Sci Technol* 12:72–80
- [25] Zhuang H, Lugscheider E (1982) The deoxidation and wetting mechanism of stainless steel in vacuum brazing. *Hanjie Xuebao* 3:139–152
- [26] Asl KM, Luo J (2012) Impurity effects on the intergranular liquid bismuth penetration in polycrystalline nickel. *Acta Mater* 60:149–165
- [27] Mu GQ, Zhang YH, Qu WQ, Zhuang HS (2022) Mechanism of intergranular penetration of liquid filler metal into oxygen-free copper. *Weld World* 66:1447–1460
- [28] Savage WF, Nippes EP, Mushala MC (1978) Copper contamination cracking in the weld heat-affected zone. *Weld J* 57:145s–152s
- [29] Asnis EA, Prokhorenko VM (1965) Mechanism of cracking during the welding or depositing of copper onto steel. *Svar Proizvod* 11:8–9
- [30] Bredzes N, Schwartzbart (1956) *Fundamentals of brazing*. Report to frankford arsenal, pp 12–14
- [31] Savage WF, Nippes EF, Stanton RP (1978) Intergranular attack of steel by molten copper. *Weld J* 57(1):9s–16s
- [32] Bozhko AM (1968) Mechanism by which molten copper penetrates into steel. *Art Svaka* 6:23–25
- [33] Chen SH, Yu XH, Huang JH, Yang J, Lin SB (2019) Interfacial ferrite band formation to suppress intergranular

- liquid copper penetration of solid steel. *J Alloys Compd* 773:719–729
- [34] Sun QJ, Jin P, Liu YB, Li JZ, Wang JF, Ma T, Feng JC (2019) Wetting of liquid copper on TC4 titanium alloy and 304 stainless steel at 1273–1433 K. *Mater Design* 169:107667
- [35] Silze F, Wiehl G, Kaban I, Kuhn U, Eckert J, Pauly S (2015) Effect of Ga on the Wettability of CuGa10 on 304L Steel. *Metall Mater Trans B* 46:1647–1653
- [36] Silze F, Wiehl G, Kaban I, Wendrock H, Gemming T, Kühn U, Eckert J, Pauly S (2016) Wetting behaviour of Cu-Ga alloys on 304L steel. *Mater Design* 91:11–18
- [37] Chen Y, Wu QQ, Pei YY, Deng J, Long WM, Liu SX (2015) Effects of brazing filler and method on ITER thermal anchor joint crack. *Mater Manuf Process* 30:1074–1079
- [38] Lee HW, Sung JH (2005) Effect of weld metal copper content on HAZ cracking in austenitic stainless steel welded with Al brass. *Sci Technol Weld Joi* 10:145–148
- [39] Shajan N, Arora KS, Shome M, Singh P, Santhanagopalan V (2020) Effect of boron in suppressing the liquid metal embrittlement in drawable grade of steel. *Sci Technol Weld Joi* 26:130–135
- [40] Joseph B, Picat M, Barbier F (1999) Liquid metal embrittlement: a state-of-the-art appraisal. *Eur Phys J AP* 5:19–31
- [41] Fredriksson H, Hansson K, Olsson A (2001) On the mechanism of liquid copper penetration into iron grain boundaries. *Scand J Metall* 30:41–50
- [42] Takeda M, Onishi T, Nakakubo S, Fujimoto S (2009) Physical properties of iron-oxide scales on Si-containing steels at high temperature. *Mater Trans* 50:2242–2246
- [43] Pique D, Coudurier L, Eustathopoulos N (1981) Adsorption of copper at the interface between solid iron and liquid silver at 1100-degrees centigrade. *Scripta Metall* 15:165–170
- [44] Mu GQ, Qu WQ, Zhang YH, Zhuang HS (2022) Effect of Ni on grain boundary penetration in vacuum brazing of copper and stainless steel. *Weld World* 67(2):483–494
- [45] Shen YX, Li ZL, Hao CY, Zhang JS (2012) A novel approach to brazing C/C composite to Ni based superalloy using alumina interlayer. *J Eur Ceram Soc* 32:1769–1774

Publisher's Note Springer Nature remains neutral with regard to jurisdictional claims in published maps and institutional affiliations.

Springer Nature or its licensor (e.g. a society or other partner) holds exclusive rights to this article under a publishing agreement with the author(s) or other rightsholder(s); author self-archiving of the accepted manuscript version of this article is solely governed by the terms of such publishing agreement and applicable law.